Journal of Power Sources 623 (2024) 235472

Contents lists available at ScienceDirect

Journal of Power Sources

journal homepage: www.elsevier.com/locate/jpowsour

Visualization of stepwise electrode decomposition in a nail penetrated commercial lithium-ion cell using low-temperature synchrotron X-ray computed tomography

Nils Böttcher [a,b,1], Shahabeddin Dayani [a,1], Henning Markötter [a,*], Anita Schmidt [a], Julia Kowal [b], Yan Lu [c,d], Jonas Krug von Nidda [a,**], Giovanni Bruno [a]

[a] Bundesanstalt für Materialforschung und -prüfung (BAM), Unter den Eichen 87, 12205, Berlin, Germany
[b] Institut für Energie- und Automatisierungstechnik, Technische Universität Berlin, Einsteinufer 11, 10587, Berlin, Germany
[c] Institute of Electrochemical Energy Storage, Helmholtz-Zentrum Berlin für Materialien und Energie, Hahn-Meitner-Platz 1, 14109, Berlin, Germany
[d] Institute for Technical and Environmental Chemistry, Friedrich-Schiller-Universität Jena, Philosophenweg 7a, 07743, Jena, Germany

HIGHLIGHTS

- 3D study of critically damaged LiB cells at low temperature.
- Synchrotron tomography at low temperatures during thermal runaway.
- Correlation between structural features and temperature changes demonstrated.

ABSTRACT

The transition towards zero carbon emissions in power generation hinges on the integration of efficient electrical energy storage systems, with lithium-ion batteries (LIBs) positioned as a pivotal technology. While generally safe, deviations in their operational guidelines due to manufacturing defects or misuse can lead to critical safety concerns, notably thermal runaway (TR) events. Internal short circuits (ISCs) are primary initiators of TR within LIBs. For abuse testing, ISCs are often triggered by nail penetration. This study explores the morphological changes and mechanisms underlying ISC-induced TR in LIBs using operando synchrotron X-ray computed tomography (SXCT) at subzero temperatures. A novel cryogenic setup was developed to control a stepwise temperature increase in the damaged sample while monitoring electrochemical characteristics and simultaneously enabling acquisition of high-resolution SXCT images. The findings reveal that conducting nail penetration at minus 80 °C prevents immediate TR, enabling detailed analysis of subsequent structural and electrochemical behavior during controlled thawing. Thus, the initiation of TR processes at localized ISC sites has been observed, evidenced by voltage fluctuations and morphological changes, such as cathode material cracking and decomposition. These results underscore the importance of temperature control in mitigating TR risks and provide critical insights into the internal dynamics of LIBs under abusive conditions. The developed cryogenic SXCT methodology offers a powerful tool for non-destructive, high-resolution investigation of battery failure mechanisms, contributing to the enhancement of LIB safety.

1. Introduction

The integration of electrical energy storage systems is vital for progressing towards a power generation system with zero carbon emissions. Lithium-ion batteries (LIBs), among various storage technologies, are anticipated to become the key player in the coming decades. Generally, LIBs are safe when operated within their recommended thermal, electrical, and mechanical guidelines. Nevertheless, deviations due to manufacturing errors or improper use can lead to unexpected safety challenges over time [1]. It is important to note that critically damaged LIBs can lead to severe consequences, particularly when a thermal runaway (TR) occurs.

Thermal runaways occur when a rise in temperature triggers an exothermic reaction, resulting in the release of additional energy, which in turn initiates an uncontrolled chain reaction. In LIBs, it describes a situation where an exothermic reaction exceeds safe limits, causing

* Corresponding author.
** Corresponding author.
E-mail addresses: henning.markoetter@bam.de (H. Markötter), Jonas.Krug-von-nidda@bam.de (J. Krug von Nidda).
[1] these authors contributed equally to this work.

https://doi.org/10.1016/j.jpowsour.2024.235472
Received 18 June 2024; Received in revised form 26 August 2024; Accepted 15 September 2024
Available online 25 September 2024

temperatures to rise uncontrollably. Börger et al. [2] portrays various scenarios of such reactions, differentiating between abnormal heating that can be mitigated by cooling, and progressive heating that, once initiated, is unstoppable and may result in catastrophic outcomes.

Considerable effort has been invested in studying, standardizing, and regulating various abuse tests for LIBs. This is essential for inducing different safety-critical scenarios by subjecting batteries to extreme conditions which might lead to a TR [3].

In LIBs, TR events can be triggered in different ways, such as release of electrochemical energy stored within the cell through mechanical [4] or electrical abuse [5] and input of external energy in the form of heat or electrical energy [6]. These triggers can initiate or exacerbate the exothermic reactions within the battery, potentially leading to a cascade of reactions resulting in a thermal runaway if not managed effectively.

Nail penetration into a lithium-ion cell can trigger short circuits, resulting in the rapid release of stored electrochemical energy and, potentially, a thermal runaway. These short circuits are typically discussed as internal short circuits (ISCs).

ISCs involve the disruption of internal components within the cell itself. They can be sub-categorized into 4 types [7]: Type 1) between anodic (typically, copper) and cathodic (typically, aluminum) current collectors; type 2) between cathodic current collector and anode material, type 3) between anodic current collector and cathode active material, and type 4) between active materials of both electrodes. The first and second scenario are the most dangerous as they result in a low ohmic short circuit (SC). Contrarily, Type 3 and 4 can be regarded as less severe, due to the comparably low electric conductivity of the cathode active material layer. Among all, the second scenario can be considered the most malignant, especially at a fully charged state. In fact, the anodic electrode's low thermal conductivity leads to local high temperatures and, thus, increases the risk of a TR [7–9].

Researchers have devised multiple methods to induce internal short circuits in LIBs for study purposes [8,10,11]. These include mechanical deformation techniques such as indentation or nail penetration (NP), the insertion of metallic particles such as nickel or tin, or the use of a shape memory alloy between electrode layers. Another innovative approach involves inserting a low-melting point conductive wax in a desired location of the jelly roll. Such wax creates a short circuit upon melting. Currently, researchers have introduced a pair of metal pads within the cell structure to induce all four types of ICS, eliminating the need to heat the cell, thus avoiding the alteration of its electrochemical performance [9].

Nail penetration serves as a well-established method for assessing the safety of batteries, since it causes a rather harsh mechanical damage. Thus, it can stand as an example for one of the most severe scenarios in different incidents (e.g., car accidents). Yet reproducibility of test results is proven to be notably intricate due to the existence of numerous test parameters, e.g., nail morphology, nail material and penetration position. Hence, different standards have been developed to handle these challenges, such as SAE J2464 and ECE-Trans-100. They define parameters for the shape of the nail and its penetration speed [3,12–14].

In-situ electrical sensing and post-mortem analysis of the cell using imaging and analytical methods, such as, SEM, EDX, optical photography, and even laboratory based X-ray computed tomography (XCT), have been used to study short circuits in lithium-ion batteries [15]. However, to gain a detailed understanding of the underlying mechanisms of critical scenarios, one needs to employ a possibly non-invasive and in-situ method. Although very challenging, synchrotron X-ray imaging has been employed in different investigations to non-destructively visualize how an internal short circuit might lead to critical damages or even to a TR. For example, the initiation and propagation of an internal short circuit in an 18650 cell were captured using synchrotron X-ray radiography when an aluminum-to-graphite short circuit was initiated [11]. In another study, high-speed synchrotron X-ray computed tomography (XCT) and radiography, combined with thermal imaging, were utilized to explore the internal structural damage and the thermal behavior during a TR in a LIB 18650-cell with lithium nickel manganese cobalt oxide (NMC) as positive electrode active material. The study revealed crucial degradation modes such as gas-induced delamination, electrode layer collapse, and the propagation of structural degradation [16].

Given that TR is an exceedingly rapid event, even the quickest XCT technology struggle to capture the phenomenon and its mechanisms in 3D with precise detail. While it is known that TR can be initiated at room temperature in most of the current LIB cell types, several publications indicate that abusing identical cells at temperatures below 0 °C can effectively prevent a TR [17–19]. Research conducted by Nandini et al. [20] demonstrates that complete immersion of a LIB-cell in liquid nitrogen results in a voltage drop to 0 V, indicating complete inertization of the cell.

During a NP test, the conductivity of the nail and the extent of damage it causes are significant factors influencing the occurrence of a TR [21]. A study of Böttcher et al. demonstrated that removing the nail from a commercial LIB-cell at −80 °C successfully prevents a TR during its subsequent re-thermalization to room temperature. Moreover, if the nail is removed at −80 °C, even a voltage recovery during the thawing process can be observed. However, such a cell experiences slow self-discharge after being fully thawed, suggesting persistent reactions stemming from nail-induced damage. This noteworthy discovery needs additional examination, especially using methods that can show details at the electrode level.

Therefore, the innovative approach of conducting XCT at subzero temperatures was considered. This method aims to decelerate the reaction or potentially halt the TR-process at certain stages, offering a novel perspective on studying this fast-acting phenomenon in greater detail.

XCT studies at temperatures different from the ambient present unique challenges. The duration of an XCT scan of a battery is usually between a few seconds to several hours, depending on factors such as type of X-ray source, properties of the material under examination, and desired resolution [22]. To obtain high resolution and noise free XCT images, it is essential to control any morphological changes in the sample during the scanning process. Such changes can cause motion blur, leading to strong image artifacts. Consequently, performing XCT scans of samples in non-equilibrium conditions is a complex task, which requires careful planning.

Despite the above-discussed challenges, there have been successful instances of employing XCT imaging in environments with temperatures ranging from slightly below 0 °C to as low as −150 °C. For example, XCT was used to characterize ice formation at −18 ± 2 °C in jet A-1 fuel, demonstrating the technology's capability in cold environments. Additionally, an investigation of the methane hydrate growth dynamics in porous media has employed XCT under similar temperature conditions [23,24].

The present study couples operando synchrotron X-ray computed tomography (SXCT) with thermal and electrochemical measurements. The goal was to explore the relationship between morphological changes and temperature as well as voltage features in a commercial LIB-cell during internal short circuit-induced failure. A specialized setup was developed to enable subzero temperature controlled SXCT of battery cells. First, digital volume correlation (DVC) was utilized to study the impact of significant temperature change on jelly roll deformation in an undamaged cell. By damaging a LIB-cell at subzero temperatures, severe reactions caused by internal short circuits were prevented, allowing a careful examination of electrode decomposition through controlled stepwise thawing during subsequent SXCT-experiments. Concurrence between morphological changes in the cathode layer and the voltage of the cell was observed. The occurrence of the first voltage peak upon thawing was linked to a visible crack formation in the cathode layer. Moreover, cathode decomposition on edges of the nail penetrated area indicated initiation of local TR-processes.

1.1. A dedicated cryogenic setup for operando XCT

An overview of the designed Cryo-LIB-SXCT setup is shown in Fig. 1a. The setup allows to cool and monitor temperature as well as electrochemical features of a LIB-cell while simultaneously capturing X-ray images during operation. The low temperature in the cold chamber is achieved by a cold gas generator (components 1 to 4) that evaporates liquid nitrogen using a jet heater element with a fixed flow (up to 2 l s^{-1}). The gas heater element, installed in the vacuum insulated hose, provides the desired nitrogen gas temperature and flow. The cold chamber is made of polyether ether ketone (PEEK), since this material can withstand low temperatures down to −190 °C as well as high temperatures up to 350 °C. Furthermore, PEEK is almost transparent to x-rays (low attenuation coefficient).

To have a better understanding of the sample environment of the cell, three additional type-K thermocouples were installed in the cold chamber (Fig. 1b). Due to the necessity of rotating the LIB-cell while acquiring projections for SXCT, all measured electrical signals need to be passed through the slip-ring of the rotating table [25]. To avoid obstruction of X-rays, all connectors are designed to pass beneath the LIB-cell, except for the type-K thermocouples, which are guided from above into the cold chamber. Moreover, in order to prevent damage to the sensitive SXCT equipment, a fire-resistant plate of calcium silicate is placed below the device under test (DUT).

Fig. 1c depicts the sample exchange position of the cold chamber. By moving the cold chamber up, while nitrogen flow passes through the chamber, a pair of magnetic connectors enables self-aligning positioning of the DUT. Hence, mounting a sample is possible within seconds. This is important if the prepared sample needs to be kept at sub-zero temperatures. This system is hereinafter referred to as quick-change connector (QCC). The magnetic cell holder has 6 electrical contacts, enabling the connection with the PT1000 temperature sensor and the 4-wire electrical connection. Moreover, a commercial USB-C breakout board and a magnetic USB-C charge connector were used to support the simplicity and cost effectiveness of the developed set-up.

Fig. 1d shows a DUT exemplarily placed below the cold chamber and two nozzles directed on the cold chamber surface. From these nozzles dry air flows around the cold chamber, preventing ice formation on the outside of the cold chamber during low-temperature testing.

In order to capture tomographic images of a commercial LIB-cell with electrode details, a rather small cell with dimensions of 8x8x4mm (width x height x thickness) was chosen, based on prior

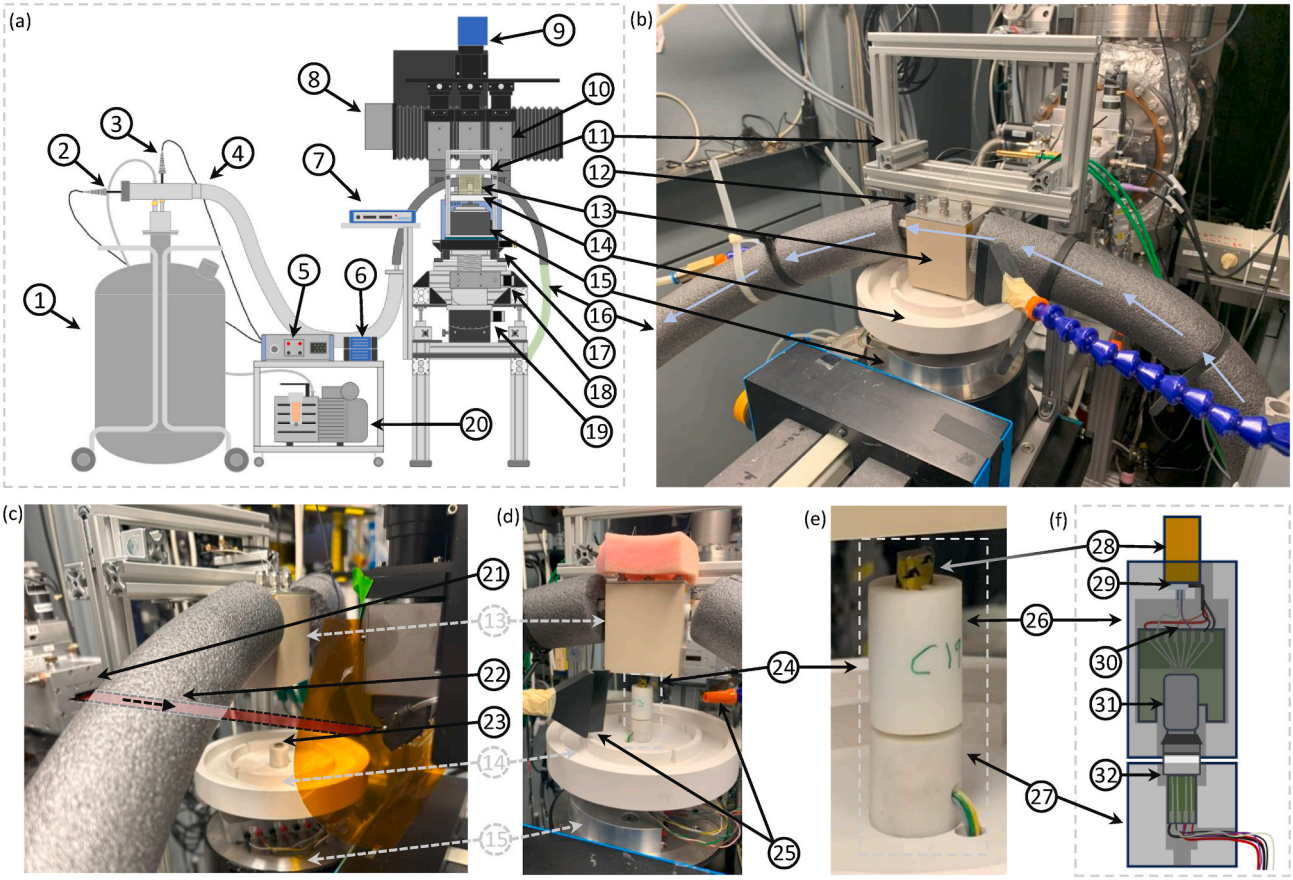

1.	LN_2 vessel	9.	Camera	17.	CT-Table x-axis control	25.	Dried pressure air
2.	Cold gas jet	10.	Magnification lenses (2x 5x 10x)	18.	CT-Table z-axis control	26.	sample holder
3.	Cold gas heater	11.	Cooled chamber bracket	19.	CT-Table angle control	27.	3d printed housing
4.	Cold gas vacuum isolated hose	12.	Typ-k temperature sensors	20.	Vacuum pump	28.	Cell sample
5.	Cold gas control unit	13.	Cold chamber	21.	SXR beam source	29.	PT1000 sensor
6.	Temperature and voltage acquisition	14.	Calcium silicate heat shield	22.	Schematic SXCT beam	30.	4-wire cell connection
7.	Potentiostat	15.	Turntable with slipring	23.	Quick-change connector	31.	USB-C circuit board
8.	Synchrotron X-Ray (SXR) Detector	16.	Cold gas hose with nitrogen flow	24.	Sample holder	32.	Magnetic circuit board

Fig. 1. – Setup Overview –Cryo-LIB-SXCT description of the setup in detail. a) Schematic view of the setup including the SXCT detector. b) Flow of inlet gas into the X-ray transparent cold chamber. c) Levitated cold chamber for quick sample exchange. d) Sample installed on the rotating table. e) Sample and sample holder. f) Details of sample holder with break board connecting all signals from the cell to the equipment.

research by Dayani et al. [22].

Fig. 1e and f show the newly designed (and 3D printed) cell holder with the QCC system. The integrated 4-wire connection also enables detailed electrochemical studies, e.g., employing electrochemical impedance spectroscopy.

2. Result and discussion

First, morphological features solely caused by a significant change in temperature (i.e., $\Delta T = 150\ ^{\circ}C$) were studied on an undamaged LIB-cell by synchrotron X-ray computed tomography. The pouch cell was scanned at 20 °C and subsequently at −130 °C. To minimize potential motion artifacts due to the cooling nitrogen stream, the scan at low temperature was performed faster. This slightly decreased the resolution. To better visualize the effects of temperature variation, the acquired XCTs were overlaid and registered at the midpoint of the cell. The SXCT at lower and at higher temperature are indicated with a blue and a red color mapping, respectively (Fig. 2b and c).

The XCT scans reveal that the cathode material remains resilient to cracking even at low temperatures although there is noticeable shrinkage across the cell, suggesting overall volume contraction. Interestingly, this volume change is not uniform and even shows unexpected expansion at different cell locations, possibly, due to the layers moving and sliding in opposite directions within the jelly roll structure.

DVC was employed to quantitatively assess the cell's movement due to temperature changes. The results, overlaid on a CT-slice in the X-Y plane, reveal anisotropic thermal contraction with extreme contraction on the north and west sides and moderate shrinkage on the south (Fig. 2a). Outer layers are more affected than inner layers, likely due to greater stress on the inner layers, resulting in higher mechanical stability. Furthermore, the presence of the tabs on the south side significantly contributes to the mechanical stability of the cell. Physically opening this cell type revealed that the entire jelly roll is secured with Kapton tape at the southern part, where the tabs are visible. Such Kapton foil potentially enhances the structural stability in that region.

Another similar cell was selected for studying sub-zero nail penetration experiment. This cell was prepared using the in-house built high precision tool at BAM [21] and was afterwards investigated in the Cryo-LIB-SXCT setup. The entire test procedure can be found in the supporting information S1. Fig. 3a visualizes the temperature and voltage during the sample preparation. Step 1 marked in Fig. 3 marks the beginning of the cooling process. The test chamber was already pre-cooled, thus the temperature of ~0 °C in the beginning. At step 2, a stable cell voltage of 0 V was reached indicating a full inertization of the

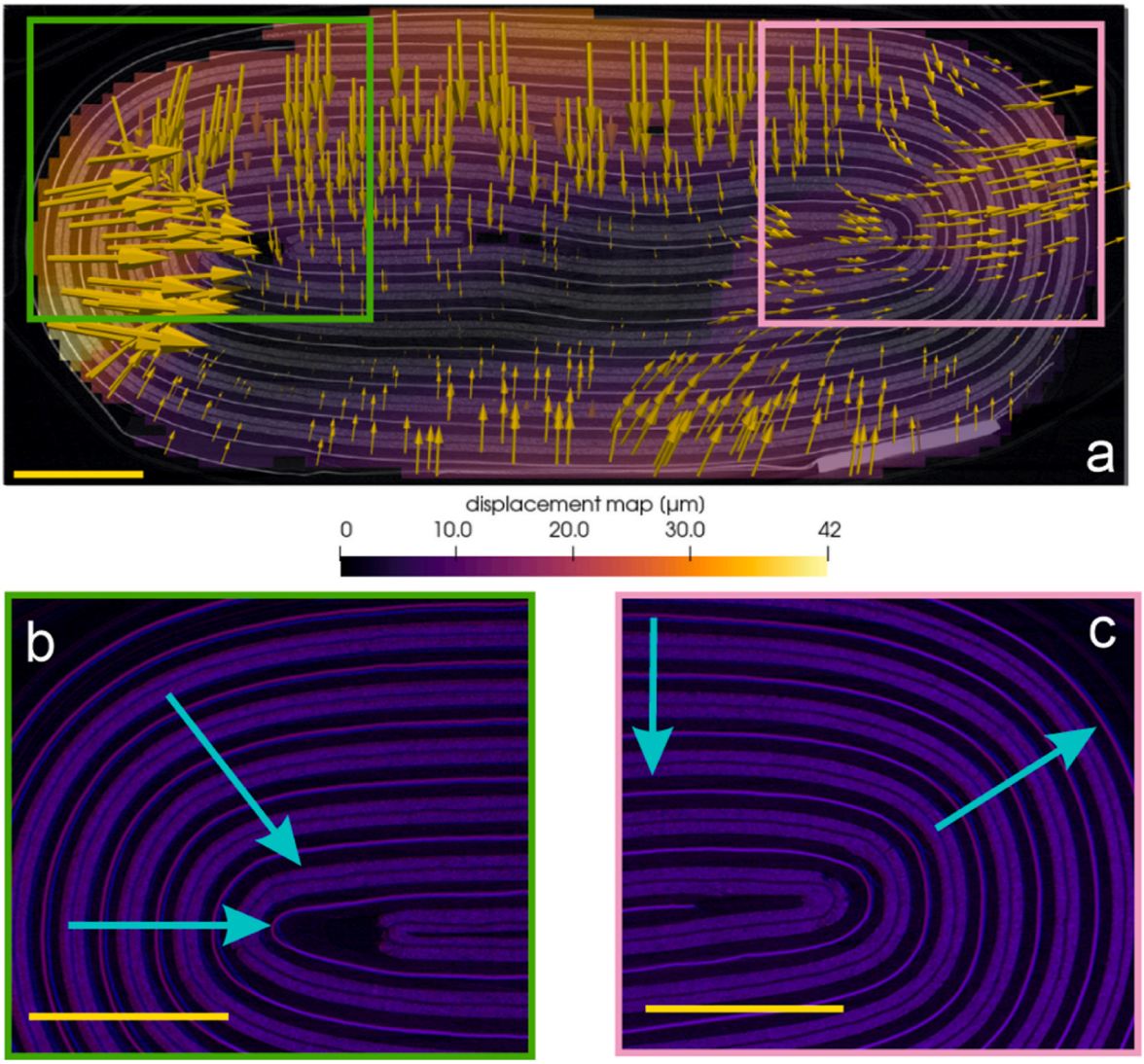

Fig. 2. – Effect of sub-zero temperature on the commercial LIB pouch cell investigated. a) Direction and magnitude of the detected displacement map using DVC overlayed on the SXCT measurement of the pouch cell. b) and c) Enlarged regions from overlayed SXCT volumes of the cell at −130 °C (blue) and +20 °C (red). Scale bars on all images equal to 1 mm. (For interpretation of the references to color in this figure legend, the reader is referred to the Web version of this article.)

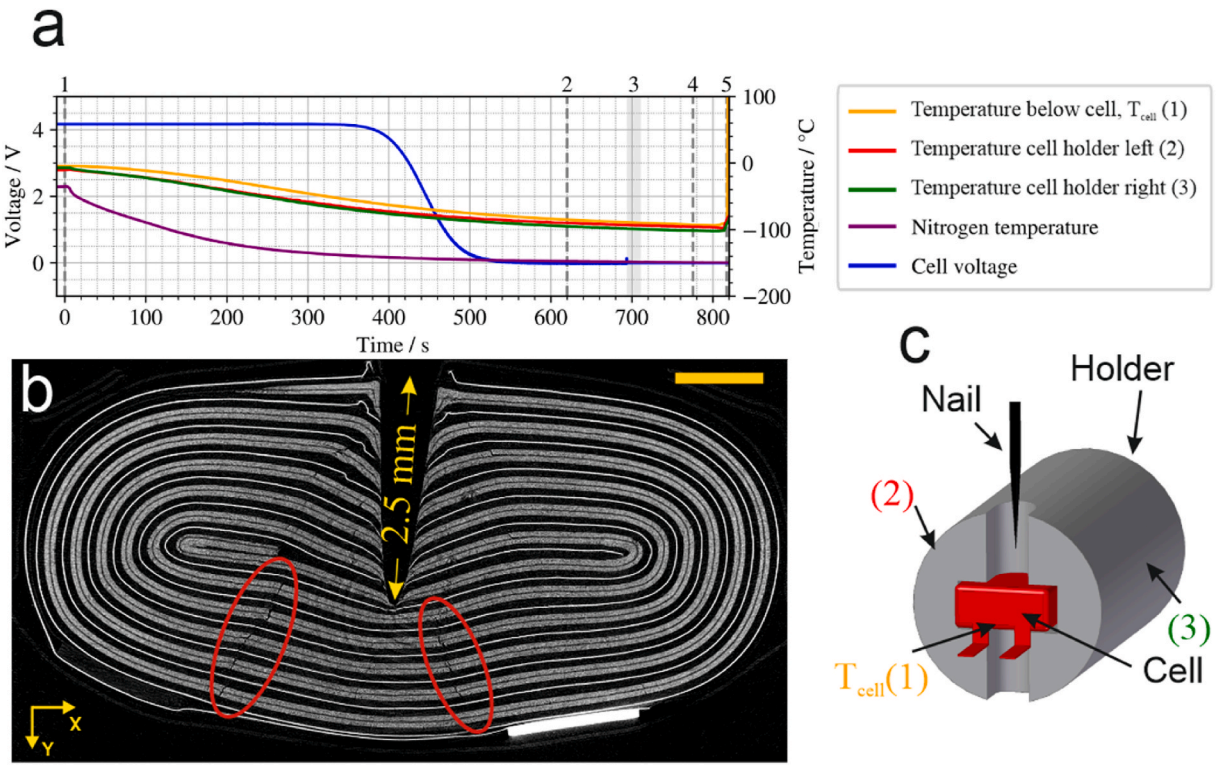

Fig. 3. Sample preparation: Nail penetration at subzero temperature. a) Voltage and temperature of the cell during the nail penetration. Different steps of the process are marked by vertical lines. b) SXCT of the cell after nail penetration. The scale bar equals 1 mm. c) Schematic illustration of the cell holder of the nail penetration set up with marked positions of the three temperature sensors.

cell. This is connected to the drastically decreased ionic conductivity of the cell at such low temperatures. Section 3 marks the nail penetration region consisting of the penetration itself - with a speed of 5 mm s^{-1} and a depth of 3 mm - and the removal of the nail. During this section, no thermal reaction occurred in the cell. This confirms the inert state of the cell at – 80 °C. In fact, the ionic conductivity of the cell is too low to allow any relevant current flux inside the cell, although the electric conductivity is given due to the presence of multiple ISCs. At step 4 the test chamber was opened.

At step 5 the cell was removed from the cell holder in a cooled state (i.e., $T_{cell} = -80$ °C). Subsequently, the sample was stored in a cryogenic vessel (CryoVessel) at approximately −180 °C. This vessel was used for the transfer of the nail penetrated cell to the experimental setup at the synchrotron facility. Fig. 3b shows the CT-image of the nail-penetrated sample using the Cryo-LIB-SXCT setup (T_{cell} at ca. −60 °C). Intriguingly, the SXCT image reveals a series of cracks in the cathode material and the curved cell jelly roll towards the lower side of the image (see red circles in Fig. 3b). Those cracks are not visible in the image of the non-penetrated cell in Fig. 2. Hence, they are a direct result of the nail penetration test. As the NP test was conducted at −80 °C, crack formation due to TR-related reactions can be excluded. Thus, the crack formation can be connected to the set-up itself. The cell holder designed for the nail penetration is depicted in Fig. 3c. The cell is placed within a specifically carved groove. Above and below the cell, a cylindrical hole is positioned, allowing the needle to enter and exit the cell in case of a complete penetration. During penetration, the cell is pushed in the trajectory of the nail's movement. Hence, significant stress is exerted on the cell's surface at the edges of the cylindrical hole. Consequently, cracks in the jelly roll tend to form along these edges. These cracks can be presumably attributed to brittleness of the electrode sheets at low temperatures.

The behaviour of the nail penetrated cell during controlled rethermalization was studied in the developed Cryo-LIB-SXCT setup in detail. During the SXCT measurements, the temperature of the cell was monitored by three sensors located within the cold chamber (identified as 6, 8 and 9 in Fig. 4) and one sensor positioned directly beneath the cell (T_{cell}, identified as 7 in Fig. 4). It needs to be considered that the absolute cell temperature may slightly deviate from the measured value (T_{cell}). Moreover, the recorded T_{cell} does not allow conclusions regarding locally occurring temperatures. The temperature and voltage readings are depicted in Fig. 4. The light blue shaded sections represent the periods where the SXCT scans were recorded. The vertical orange dashed lines mark different steps of the testing procedure.

After 30 min cooling, the DUT was placed on the cell holder (step 1 in Fig. 4). The first CT scans measured at low temperature revealed motion artifacts in reconstructions. To minimize sample movement, the gas jet was guided away from the sample at step 2. Between step 2 and step 3, various XCT imaging options were tested to optimize the resulting image quality by varying the number of projections and exposure time.

Subsequently, SXCT measurements were taken with the optimized conditions every 2.5 min to observe structural changes in the cell upon stepwise rethermalization. Each measurement involved acquiring 1000 projections with an exposure time of 150 ms per projection. Four SXCT scans are chosen to highlight the relationship between the voltage reading and morphological alterations. The respective timeframes are highlighted in green in Fig. 4. The corresponding scans are numbered with Roman numerals (I to IV) and are herein discussed as different instances of the rethermalization process. These instances represent time frames after a stepwise increase in temperature of the cooling gas stream. Correspondingly, the gained SXCT-results capture the stepwise change in the electrode morphology.

Starting from the marked step 4 in Fig. 4, the cooling gas temperature was increased with a slower rate to guarantee a controlled reheating. Up to a cell temperature of −20 °C, the cell's voltage remained constant at 0 V. However, once the temperature passed this value upon heating, the voltage exhibited a rippling pattern. Intriguingly, a single small first voltage spike of 0.2 V was detected at t = 4.5 h. This observation hints at first reactions stemming from the ISCs induced by the mechanical abuse.

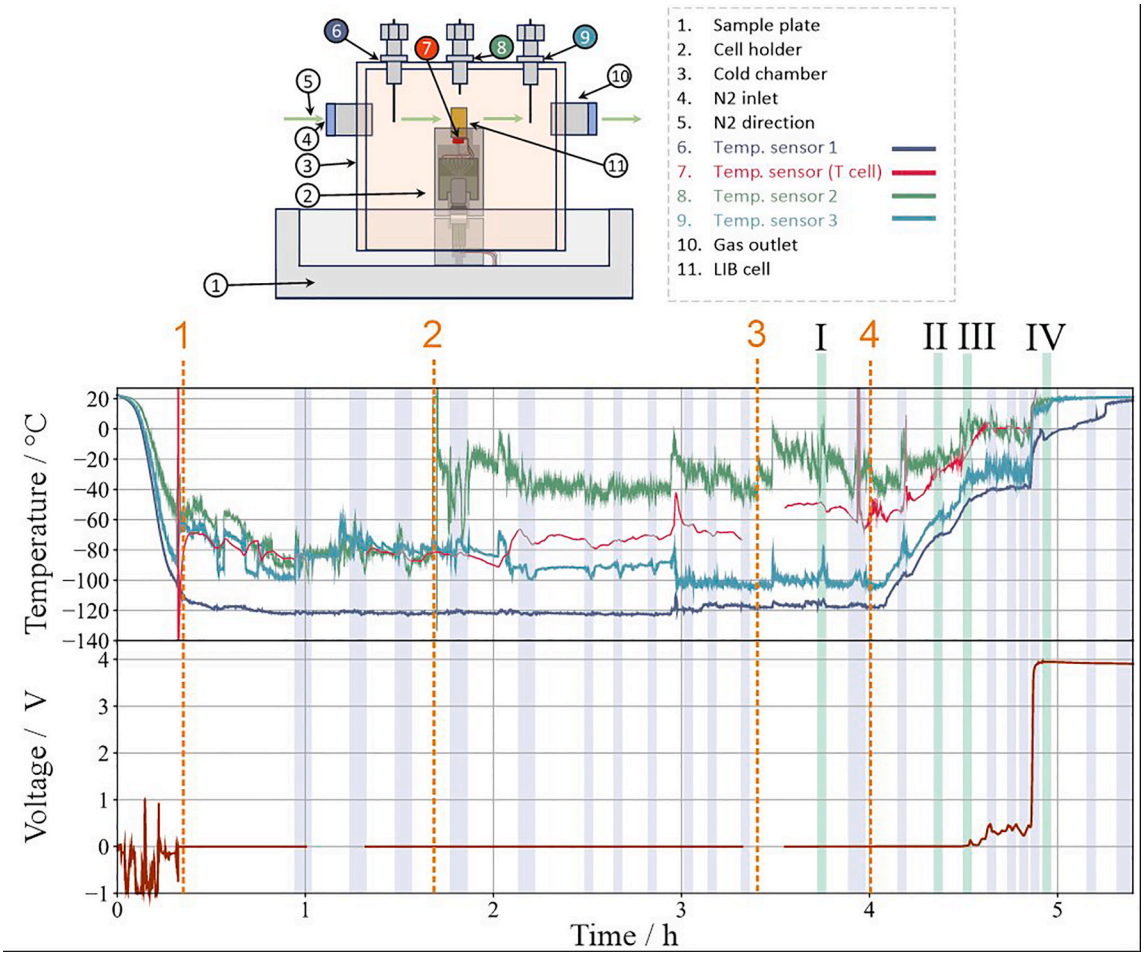

Fig. 4. –Temperature and voltage of the nail penetrated cell during rethermalization in the Cryo-LIB-SXCT-setup. Color shaded areas show duration of each SXCT measurement. Different steps of the process are marked by vertical dashed orange lines. (For interpretation of the references to color in this figure legend, the reader is referred to the Web version of this article.)

After the first voltage spike, the voltage dropped to 0.0 V again, although the recorded cell temperature continued to increase. This indicates the passivation of existing ISCs inside the cell. Further increase in cell temperature to ca. 0 °C caused more voltage fluctuations, lasting for about 20 min in total. The next controlled temperature increase led to an almost full voltage recovery of the cell. Thus, it can be assumed that most of the ISC reactions had taken place and the ISC area is in a passivated state. During this process the cell temperature signal was lost. Nonetheless, the other temperature sensors in the cold chamber (identified as 6, 8 and 9 in Fig. 4) and following SXCT scans clearly show that no global TR reactions occurred.

After being reheated to room temperature, the cell experienced a slow self-discharge, eventually showing a voltage of 0 V after several days. Apparently, some high-ohmic ISCs are still present in the cell, enabling a gradual discharge.

Further insights regarding damage induced reactions during rethermalization are gained from the analysis of selected SXCT images. Starting from the completely inert state in instance I, no structural changes are visible until the cell temperature reached a stable value of −30 °C in instance II (see Figure S2). Instance II and III were deliberately selected to discuss changes induced by the first observed voltage spike at t = 4.5 h. To facilitate a more accurate comparison of the changes inside the cell, instance II was aligned with instance III. As seen in Fig. 2, thermal expansion prevented complete overlay of all sections of the two instances. However, registration was achieved for most parts of the volume. Thus, the alignment of selected corresponding regions could enable quantitative analysis.

Fig. 5 depicts the corresponding tomographic slices of instance II and III. Fig. 5a–c and Fig. 5d–f correspond to instance II and III, respectively. In the top row (Fig. 5a and d), the volume is sliced to display a Z-Y view of the cell, revealing features such as the hole resulting from the NP, the damaged copper current collector, and the adjacent cathode electrodes. Within Fig. 5d (instance III), two regions are highlighted in orange and purple, indicating defects in the cathode material that are absent in instances at lower temperatures (i.e., instance I and II). The opening created by the nail is equidistant to both highlighted regions. Fig. 5b and e, and Fig. 5c and f depict X-Y slices indicated by dotted red and green lines in Fig. 5a and d. The corresponding images of instance III clearly reveal that the defects highlighted in Fig. 5d can be connected to cracks in the cathode electrode layer.

Interestingly, the crack formation in the cathode electrode layer depicted in Fig. 5 (instance III) correlates with the appearance of the first voltage spike shown in Fig. 5. The raising voltage indicates that sufficient ionic transport is possible at this temperature, leading to high internal currents. As a result, localized joule heating can be a potential reason for local TR-processes in the cell. The subsequent drop in voltage hints limitations in current flow. This cannot be due to a decrease in ionic conductivity since T_{cell} is simultaneously increasing. Therefore, partial passivation or activation of the ISCs have caused changes in electrical conductivity.

The observed crack formation in the cathode electrode in instance III can be attributed to several thermal effects: i) thermal expansion or stress due to inhomogeneous thawing of the cell (as shown in Fig. 2), ii) temperature-induced change of materials' properties (e.g., phase

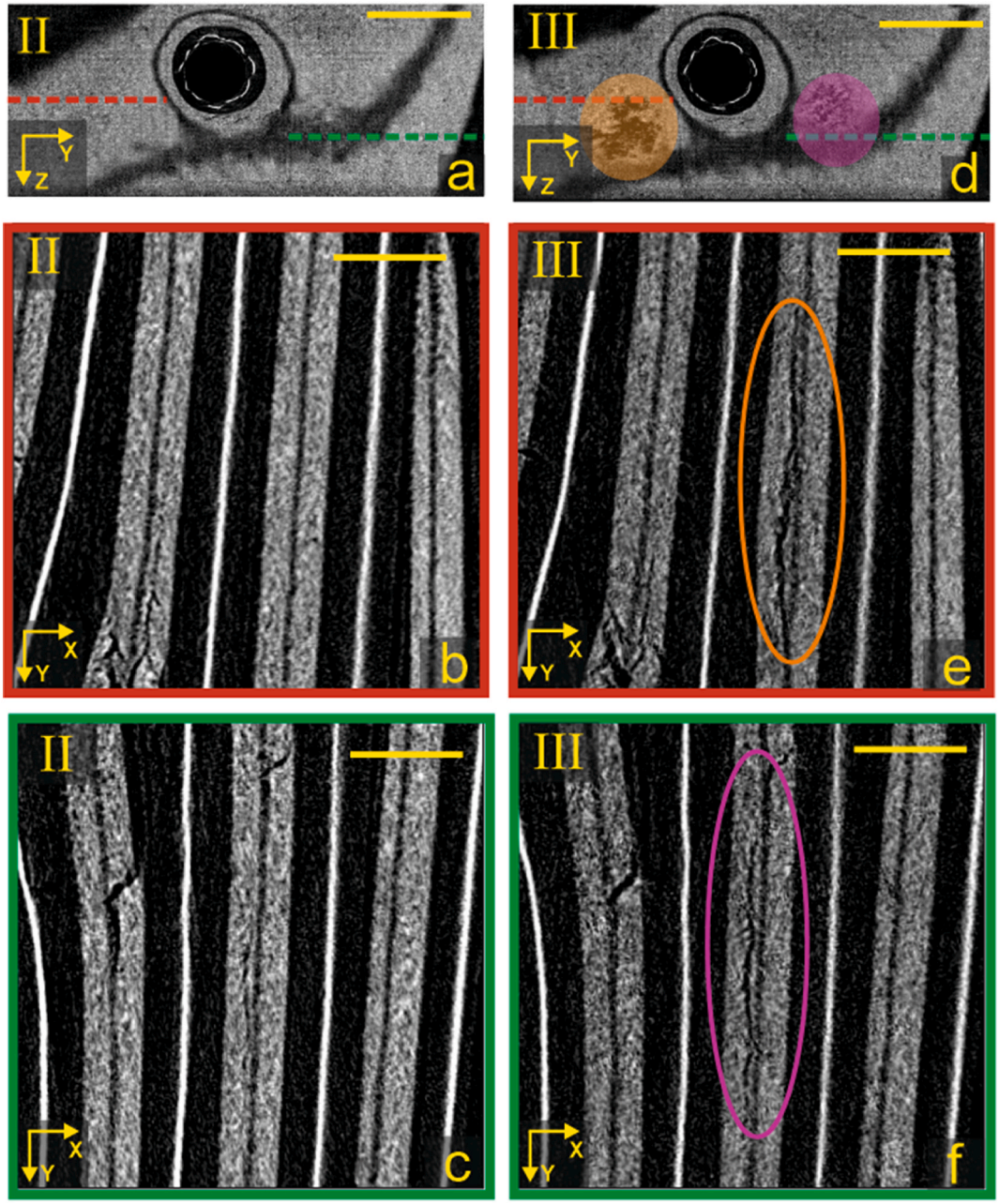

Fig. 5. – SXCT of the nail penetrated cell at instance II and III. Marked regions on the second column identify crack formation in the cathode electrode during the rethermalization process. The scale bar in a and d equals 1 mm and in the rest of the images 250 μm.

changes), or iii) locally restricted, initial TR-processes coupled with gas formation. The cell surface temperatures recorded for instances II and III were −30 °C and −20 °C, respectively. While this may present a narrow temperature variance, the presence of locally restricted TR processes leading to the formation of local hotspots can significantly widen this range, potentially amplifying the impact of both i) and ii).

To gain further insights on the processes during rethermalization, the edges of the hole created by the nail are compared for the different instances. This region can visualize the ISCs created by the nail penetration. Going from instance I to III, no changes are visible in this region (see Fig. S3). All three instances reveal smooth edges and bended electrode layers in the trajectory of the nail. The first clear change is visible when comparing instances III and IV (see Fig. 6). Instance III represents the state at the first voltage spike, marking the initial start of TR-processes at $T_{cell} = -20$ °C. The SXCT at instance IV is measured after the final stepwise temperature increase where the cell voltage rapidly increased to 3.9 V. Comparing instances III and IV in Fig. 6, the cathode material has disappeared at the edges created by the nail. This loss of cathode active material can be connected the initiation of TR at the edges and contributes to the aforementioned passivation of ISCs. Furthermore, this is accompanied by bending and deformation of the electrode layers at the nail edges.

Generally, the images in Fig. 6 support the abovementioned assumption that the appearance of voltage fluctuations can be connected to local TR-processes. The fluctuations in voltage, i.e., voltage ripples, between instances III and IV suggest the continuous change in apparent resistance inside the cell. This can be related to local variations in temperature or alterations in ionic as well as electric conductivity pathways. All these effects can be caused by decomposition reactions. It is worth noting that in all marked regions in Fig. 6a, there may be an aluminum-to-copper or aluminum-to-anode short circuit. However, due to the low temperature as well as the low capacity of the cell, not enough

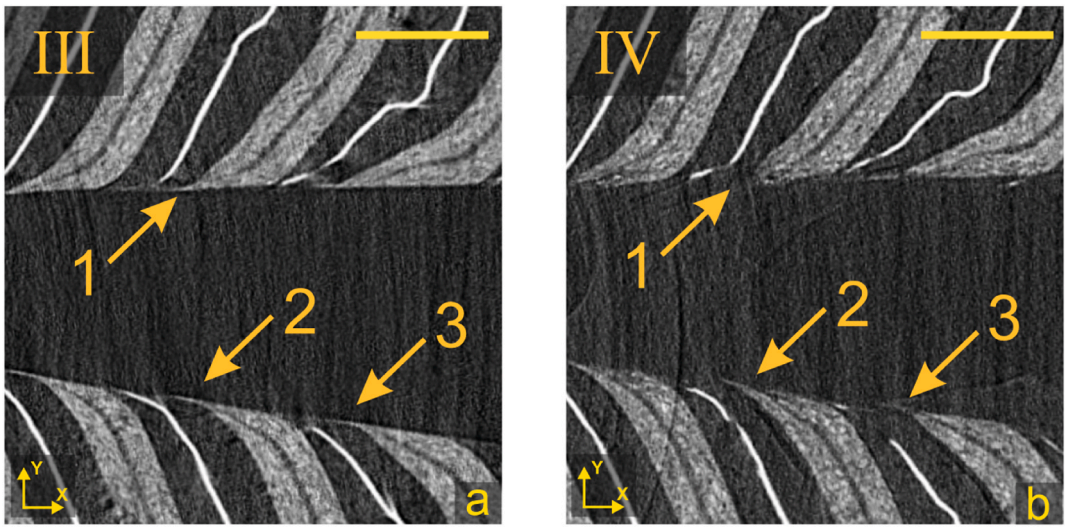

Fig. 6. SXCT of the nail penetrated cell at a) instance III and b) instance IV. Comparing marked spots (1, 2, 3) visualizes that the cathode active material has reacted at the edge of the trace of the nail. Scale bar equals 250 μm.

heat was generated to trigger a TR at the global scale. It can be speculated that the cathode material reacted and decomposed because of these short circuits. Presumably, a TR started locally at the ISC spots resulting in local hot spots accompanied with gas formation. Hence, the cathode layer was partially spalled in these regions.

The occurrence of cathode decomposition during rethermalization serves as indirect evidence that the sample had remained at non-reacting temperatures since its preparation. Since the reactions discussed above are irreversible, they occurred for the first time during the operando investigations.

In the event of nail penetration, all four types of internal short circuits - as outlined in the introduction - are expected to occur, with type 1 and type 2 being the most catastrophic. However, if the nail is removed after penetration, existing short circuits primarily affect small volumes. Consequently, the propagation of thermal events is hindered as the exchange of electrons and ions is confined to such small volumes. This prevents substantial heat generation (at the global scale) from decomposition reactions. Moreover, the existing ISCs seem to be passivated upon further thawing. This phenomenon can be connected to various thermal effects, e.g., spalling of electrode layers or thermal expansion of current collectors. The latter should be rather easy in damaged areas, once the nail is extracted from the cell. At the end of the test, only small ISCs seem to be present. Such ISCs cause a slow self-discharge rate of the abused cell. Generally, the present results support the findings of Böttcher et al. [21]: The presence of the nail in the cell during the thawing process seems to be a crucial step for the initiation of a TR. Similar findings were found during room temperature nail penetration tests, just before cell-wide TR, as investigated with high-speed synchrotron X-ray radiography by Finegan et al. [26]. Moreover, the possibility that the described effects, e.g., spalling of electrodes and bending of current collectors, can avoid a cell-wide TR were also seen during the nail penetration of LIB-cells with a coated polymer current collector [27]. Apparently, both strategies, i.e., nail removal at low temperatures as well as polymer current collectors, allow to locally restrict the effects of the nail penetration or even the TR itself.

While the above-mentioned analysis of the observed morphological changes is reasonable, further quantitative analysis of the entire volume is necessary. Possibly, there are morphological alterations that went unnoticed due to thermal expansion and subsequent movement of the jelly roll (the resolution and the field of view of XCT are limited). In order to quantitatively analyze and compare images, reliable and precise image registration of the analyzed region is essential. Due to non-rigid movements caused by thermal differences, registration of the entire volume is impractical. Hence, the authors recommend further exploration of the valuable recorded dataset using DVC. Implementing DVC on all volumes, comparing them to the initial recorded volume, and deforming the volumes using the resulting displacement field allow image overlay. Using DVC, a comprehensive analysis of morphological changes across the recorded volumes would be enabled. Such an analysis lays beyond the scope of the present work but will be addressed in the future.

3. Conclusion

The primary focus of this work was to investigate battery cells under operating conditions at temperatures ranging between −130 and 20 °C. To this aim, a Cryo-LIB-SXCT setup was developed to investigate the morphological and electrical changes occurring during rethermalization of a LIB-cell, critically damaged at - 80 °C.

Valuable insights into the effects of low temperatures on commercial LIB-cells, particularly in relation to NP-induced thermal runaway and mechanical stability of the jelly roll, were gained using operando SXCT. Non-uniform thermal contraction within an undamaged cell was visualized and quantified using DVC. Another cell was penetrated with a nail and was initially held at low temperatures to hinder the occurrence of TR-related reactions. By performing operando SXCT during the stepwise rethermalization of the pre-damaged cell, it was possible to demonstrate correlations between morphological changes in the cathode layer and cell voltage. In fact, the voltage footprint can be used to detect the onset of first TR-related crack formations inside the cell.

Cathode decomposition was observed during operando investigations. The first SXCT scans indicated that no TR-related reactions occurred in the cell after NP at low temperatures and from the testing procedure (T_{cell} maximum ca. −40 °C before controlled rethermalization). Nail penetration was found to cause internal short circuits; however, removal of the nail at low temperatures limited their impact to small volumes, reducing heat generation throughout the whole cell upon the subsequent rethermalization. During the thawing process, existing short-circuits were mitigated or passivated by thermal effects. In fact, it was found that TR-processes induced spalling of the electrode layers or bending of aluminum and copper current collectors, presumably caused by thermal expansion. These results support previous findings that removal of the conductive nail after NP at low temperature highly reduces the risk of a TR during subsequent rethermalization [21].The Cryo-LIB-SXCT setup helped to link the occurrence of the first voltage spike at −20 °C to the first visible morphological changes inside the

cathode layer. At the end of the test, the voltage of the damaged cell was almost completely recovered. This recovery indicates the disappearance or at least the passivation of the existing short circuits. Further quantitative analysis using DVC was identified to be crucial for future in-depth investigations regarding i) the impact of initiated cracks on TR-initiation, ii) the quantification of reacted cathode material at the nail interface, iii) the identification of potential reactions within the bulk of the cathode material, and iv) the visualization of the distribution of these reactions in the 3D volume.

4. Experimental and methods

4.1. Sample information

A commercial pouch cell containing NMC532 as the cathode active material with a nominal capacity of 40 mAh was utilized for the experiments. The dimensions of the cells are $8 \times 8 \times 4$ mm^3

4.2. Low temperature operando SXCT imaging

Synchrotron X-ray computed tomography was performed at the imaging station of BAM*line* (operated by BAM), located in the BESSY II synchrotron facility operated by the Helmholtz-Zentrum Berlin (HZB) [22,25].

A custom-made set-up (introduced in Fig. 1) was designed and built to control the temperature of the sample while performing synchrotron X-ray computer tomography. Imaging parameters were the following: Projections were acquired using a parallel monochromatic X-ray beam with an energy of 48 keV and an energy resolution of ~3.5 %. Effective pixel size of the detector was 3.6 μm. The rotating table at the BAM*line* imaging set up is equipped with a slip-ring, which facilitates the continuous connection of the cell and temperature sensors during sample rotation. SXCT measurements were acquired over a 180-degree rotation. The specific settings for the shown SXCT images are mentioned in the supplementary information (Table S1).

Image reconstructions were carried out using in-house developed software based on the Tomopy package [28]tailored for batch reconstruction of multiple SXCT scans, enabling efficient 4D reconstruction.

To monitor the electrical and thermal properties of the cell, two parallel measurement systems were used. In system A, cell potential and temperature were measured using a GAMRY 1010E potentiostat. For the measurement of the cell temperature in system A, a PT1000 sensor was connected to the potentiostat. In system B, the temperature of the cold chamber and the cell voltage were monitored in a LabVIEW program. For the temperature measurements in system B, type-K thermocouples were used. In order to synchronize the data of system A with the data of system B, digital input and output signals were used.

The cooling of the cold chamber and the cell was realized with N_2 gas using a cold gas generator (*KGW-Isotherm* Type: TG-LKF-H 63/50) with a heater power of 630 W and a jet power of 500 W. The system guarantees a temperature stability of the produced cold gas within a range of ± 0.2 °C and a designated temperature output range from −180 °C to +100 °C.

4.3. Data analysis

The reconstructed tomograms were analyzed using ImageJ, Dragonfly [29] and in-house-written python scripts. Digital volume correlation was performed using the open-source SPAM software's regular grid local DIC (digital image correlation) script [30].

4.4. Nail penetration test – sample preparation

The sample was cycled five times according to the manufacturer specifications, from 2.5 V to 4.2 V. A Gamry 1010E was used to perform the charge-discharge cycles with a current of 20 mA (corresponding to C-rate of 0.5 C) at room temperature. A discharge capacity of 40 mAh was measured over the five cycles.

The nail penetration of the cell was performed at $T_{cell} = -80$ °C with the high precision NP setup described in Ref. [21]. The device consists of a steel needle (diameter of 1 mm) operated at 5 mm s^{-1} speed with a final depth of 3 mm.

The cell was transferred from the NP setup into a precooled cryo vessel (voyageur 6 Dry shipper container, IATA and ADR compliant under continuous cooling). The cryo vessel can keep a temperature of ca. −186 °C for 26 days, therefore it was used to store and transport the nail penetrated cells to the imaging beamline. During storage and transport, the temperature was constantly monitored and did not show significant variation.

CRediT authorship contribution statement

Nils Böttcher: Writing – review & editing, Writing – original draft, Validation, Methodology, Investigation, Formal analysis, Data curation, Conceptualization. **Shahabeddin Dayani:** Writing – review & editing, Writing – original draft, Visualization, Software, Methodology, Investigation, Formal analysis, Data curation, Conceptualization. **Henning Markötter:** Writing – review & editing, Supervision, Software, Resources, Methodology, Funding acquisition, Formal analysis, Conceptualization. **Anita Schmidt:** Writing – review & editing, Supervision, Resources, Project administration, Funding acquisition, Conceptualization. **Julia Kowal:** Writing – review & editing, Supervision, Project administration. **Yan Lu:** Supervision, Project administration. **Jonas Krug von Nidda:** Writing – review & editing, Writing – original draft, Validation, Supervision, Resources, Methodology, Formal analysis, Conceptualization. **Giovanni Bruno:** Writing – review & editing, Supervision, Resources, Project administration.

Declaration of competing interest

The authors declare that they have no known competing financial interests or personal relationships that could have appeared to influence the work reported in this paper.

Data availability

Data will be made available on request.

Acknowledgement

We express our sincere gratitude to all who contributed to this research project: Ralf Britzke and Michael Sintschuk (both BAM) for their invaluable assistance at BAMline. Nawar Yusfi, Max Setzchen and Oliver Zeh (all BAM) for their assistance regarding the nail penetration test. BAM (Bundesanstalt für Materialforschung und -prüfung) for funding the MI PhD-projects.

Appendix A. Supplementary data

Supplementary data to this article can be found online at https://doi.org/10.1016/j.jpowsour.2024.235472.

References

[1] L. Meng, Research and analysis of electric vehicle fire accidents and review of lithium-ion battery thermal runaway mechanism, International Journal of New Developments in Engineering and Society 6 (2) (2022).
[2] A. Börger, J. Mertens, H. Wenzl, Thermal runaway and thermal runaway propagation in batteries: what do we talk about? J. Energy Storage 24 (2019).
[3] V. Ruiz, et al., A review of international abuse testing standards and regulations for lithium ion batteries in electric and hybrid electric vehicles, Renew. Sustain. Energy Rev. 81 (2018) 1427–1452.
[4] J. Lamb, C.J. Orendorff, Evaluation of mechanical abuse techniques in lithium ion batteries, J. Power Sources 247 (2014) 189–196.

[5] F. Larsson, B.-E. Mellander, Abuse by external heating, overcharge and short circuiting of commercial lithium-ion battery cells, J. Electrochem. Soc. 161 (10) (2014) A1611–A1617.
[6] R.A. Leising, et al., Abuse testing of lithium-ion batteries: characterization of the overcharge reaction of LiCoO[sub 2]/graphite cells, J. Electrochem. Soc. 148 (8) (2001).
[7] S. Santhanagopalan, P. Ramadass, J. Zhang, Analysis of internal short-circuit in a lithium ion cell, J. Power Sources 194 (1) (2009) 550–557.
[8] M. Zhang, et al., Internal short circuit trigger method for lithium-ion battery based on shape memory alloy, J. Electrochem. Soc. 164 (13) (2017) A3038–A3044.
[9] M.K. Long, S. Liu, G. Zhang, A novel method for simultaneous triggering and in situ sensing of internal short circuit in lithium-ion cells, Energy Advances 2 (12) (2023) 2018–2028.
[10] C.J. Orendorff, E.P. Roth, G. Nagasubramanian, Experimental triggers for internal short circuits in lithium-ion cells, J. Power Sources 196 (15) (2011) 6554–6558.
[11] D.P. Finegan, et al., Characterising thermal runaway within lithium-ion cells by inducing and monitoring internal short circuits, Energy Environ. Sci. 10 (6) (2017) 1377–1388.
[12] T. Yokoshima, et al., Operando analysis of thermal runaway in lithium ion battery during nail-penetration test using an X-ray inspection system, J. Electrochem. Soc. 166 (6) (2019) A1243–A1250.
[13] J. Diekmann, et al., Development of a new procedure for nail penetration of lithium-ion cells to obtain meaningful and reproducible results, J. Electrochem. Soc. 167 (9) (2020).
[14] K. Wohrl, et al., Analysis of deactivation of 18,650 lithium-ion cells in CaCl(2), tap water and demineralized water for different insertion times, Sensors 23 (8) (2023).
[15] T. Ma, et al., Mechanics-morphologic coupling studies of commercialized lithium-ion batteries under nail penetration test, J. Power Sources 437 (2019).
[16] D.P. Finegan, et al., In-operando high-speed tomography of lithium-ion batteries during thermal runaway, Nat. Commun. 6 (2015) 6924.
[17] T.R.B. Grandjean, J. Groenewald, J. Marco, The experimental evaluation of lithium ion batteries after flash cryogenic freezing, J. Energy Storage 21 (2019) 202–215.
[18] T.R.B. Grandjean, et al., Cycle life of lithium ion batteries after flash cryogenic freezing, J. Energy Storage 24 (2019).
[19] N. Sunderlin, et al., Effects of cryogenic freezing upon lithium-ion battery safety and component integrity, J. Energy Storage 63 (2023).
[20] K. Nandini, et al., Study on survivability of 18650 Lithium-ion cells at cryogenic temperatures, J. Energy Storage 17 (2018) 409–416.
[21] N. Böttcher, S. Dayani, H. Markötter, A. Bau, M. Setzchen, A. Schmidt, J. Kowal, J. Krug von Nidda, High Precision Nail-Penetration Setup for the Controlled Thermal Runaway Initiation of Lithium-Ion Cells at Very Low Temperatures, Energy Technology 12 (5) (2024) 2301379. https://doi.org/10.1002/ente.202301379.
[22] S. Dayani, et al., Multi-level X-ray computed tomography (XCT) investigations of commercial lithium-ion batteries from cell to particle level, J. Energy Storage 66 (2023).
[23] I. Haffar, et al., X-ray tomography for 3D analysis of ice particles in jet A-1 fuel, Powder Technol. 384 (2021) 200–210.
[24] P.B. Kerkar, et al., Imaging methane hydrates growth dynamics in porous media using synchrotron X-ray computed microtomography, G-cubed 15 (12) (2014) 4759–4768.
[25] H. Markötter, et al., Upgraded imaging capabilities at the BAMline (BESSY II), J. Synchrotron Radiat. 29 (2022) 1292–1298.
[26] D.P. Finegan, et al., Tracking internal temperature and structural dynamics during nail penetration of lithium-ion cells, J. Electrochem. Soc. 164 (13) (2017) A3285.
[27] M.T.M. Pham, et al., Prevention of lithium-ion battery thermal runaway using polymer-substrate current collectors, Cell Reports Physical Science 2 (3) (2021) 100360.
[28] D. Gürsoy, et al., TomoPy: a framework for the analysis of synchrotron tomographic data, J. Synchrotron Radiat. 21 (2014) 1188–1193.
[29] Dragonfly 2020.2 [computer software], Available from: http://www.theobjects.com/dragonfly, 2022.
[30] O. Stamati, et al., Spam: software for practical analysis of materials, J. Open Source Softw. 5 (51) (2020).